Journal of Operation and Automation in Power Engineering

vol. XX, no. XX, Dec. 2022, Pages: XXXX (Proofed)

http://joape.uma.ac.ir

Voltage Stability Assessment of Power System Using Line Indices with Wind System and Solar Photovoltaic Generation Integration

S.K. Gupta and S.K. Mallik*

Department of Electrical Engineering, National Institute of Technology, Patna, Bihar, India.

***Abstract*—** *Due to the exponential increase in electricity demand, the power system is being operated at its stability limit. Due to the scarcity of natural resources, the generation can not be increased. Hence, there is always a possibility of voltage collapse in the system. The voltage collapse can be predicted by a number of line stability indices available in the literature. The stress level of the power system can be mitigated by integrating renewable energy resources, such as wind and solar energy. Under heavy loading conditions, the transmission lines get stressful which can be predicted by line voltage stability indices. In this paper, three line stability indices, namely, Lmn, fast voltage stability index (FVSI), and Lqp are used to identify the most stressed lines under four types of system loadings for ensuring the corrective measure to avoid this voltage instability. These indices are being evaluated using continuation power flow. The system loadability and stability are enhanced by deploying the wind energy and solar PV generation at the most appropriate location. The integrated test system includes wind and solar energy systems at one of the most severe bus, and the performance of the system is confirmed by computing the power flow (PF) using the integrated test system's line indices and the power system analysis toolbox (PSAT). The proposed approach has been validated on IEEE 14 and 118-bus test systems in MATLAB/PSAT with the deployment of wind energy and solar energy at a suitable location.*

***Keywords*—**CPF, indices, solar PV generation, voltage collapse, wind energy.

NOMENCLATURE

δ	Power angle
λ	Loading factor
$\lambda_{\max}$	Maximum loading factor
θ_{ij}	Line impedance angle between bus i and j
P_i	Sending end real power flow
P_j	Receiving end real power flow
Q_i	Sending end reactive power flow
Q_j	Receiving end reactive power flow
X_{ij}	Line reactance bus i and j
CPF	Continuation power flow
DFIG	Doubly-fed induction generators
FVSI	Fast Voltage Stability Index
Lmn	Line stability index
Lqp	Line stability factor
NLSI	Novel line stability index
PSVSI	Power system voltage stability index
PV	Photovoltaic
RE	Renewable energy
SCIG	Squirrel cage induction generator
VC	Voltage collapse
VCPI	Voltage collapse proximity indicator
VRIsys	System voltage recovery index

Received: 02 Aug. 2023
Revised: 29 Sep. 2023
Accepted: 16 Oct. 2023
*Corresponding author:
E-mail: santoshgupta1990@gmail.com (S.K. Gupta)
DOI: 10.22098/joape.2024.13429.2028
Research Paper

1. INTRODUCTION

In the power system sector, research and development are now primarily focused on generating electrical power from renewable energy (RE) sources. Because fossil fuels have been used for generating electricity and power distribution for so long, there is a need to design, develop, and deploy sustainable and renewable energy renovation systems in order to meet the rising world electricity demand and lessen the impact of weather change. Owing to the placement of renewable energy conversion systems, sustainable alternatives, design, and development to the conventional fossil fuel-based production system, this has grown to be a key area of inquiry on a global scale. Renewable energy can be produced from naturally inexhaustible resources like the sun, wind, and water, as well as from sources that are exhaustible with proper management, such as organic waste and wood-based biomass, the warmness from the envoironment of the earth (geothermal energy), etc. An embedded power system that uses two or more different RE sources is referred to as a hybrid energy plant [1]. For several reasons, the voltage profile of the mostly buses of the whole power system gets deteriorate as the load increases to meet the counsumers electricity demand [2]. The decline in the lines' reactive power could be the cause of this. Several billions of US dollars have been financed in the advancement of RE systems in India, Europe, Japan, North America, China, and Brazil [3]. African and Middle Eastern countries are also engaged in ongoing efforts to harness the potential of renewable energy sources. Geothermal and hydroelectric sources described for a substantial portion of Kenya's installed capacity of generation. As a result, the production of and integration of renewable energy into the grid have attracted considerable local and international attention [4, 5]. The two most general non-conventional energy sources that are variable are wind and solar. Until 2023, additionally, the research [6] projects annual new offshore and onshore of more than 55 GW installations.

A voltage drop resulted in a substantial power loss in the

power system. in order to enhance the voltage magnitude, RE is combined into the current grid. Because generated power in wind and solar depends on solar contamination strength and wind speed, respectively, the main challenge with RE is volatility [7]. The generated power can be stabilized using some controllers after integrating renewable resources. The main purpose of wind farms and photovoltaics is to improve voltage instability [8]. As a result, a brand-new idea for a modern grid is emerging. Utilizing mutual digital communication, the intelligent grid is an electronically based power grid that delivers electricity to consumers. This system supports communication control, monitoring, and analysis all over the power system chain to decrease energy consumption, decrease costs, increase efficiency, and increase the dependability and transparency of the power system. in order to fix the problems with conventional electricity grids, intelligent net meters were used to create the smart grid.

Due to the variation in wind speed in entire day, the energy from the wind may vary resulting in voltage variation. Hence, the deployment of wind energy with the utility grid may present some difficult challenges. Therefore, some controllers must reduce security concerns while stabilizing the voltage level. As a result, with the aid of controllers, the entire grid system is seamlessly deployed with RE sources. Photovoltaic and wind farms are very popular renewable energy resources integrated into the grid to enhance voltage profile and power quality [9]. The analysis of voltage instability in electrical power system with substantial levels of RE penetration is covered in-depth in the literature [10]. Also, the voltage stability of electrical system deployed with diverse distributed energy resources is explored along with a number of global assessment methodologies and development strategies. The best locations and sizes for distributed generation (DG) units based on voltage stability are presented in [11] research along with approaches for improving voltage stability.

Concerns about power system utilities have prioritized stability issues over power quality problems in order to more efficiently integrate wind power and improve system performance overall [12]. The main purpose of conducting a voltage stability analysis is to identify the fault or point of voltage instability (collapse). To pinpoint the weak bus in the system, several stability indices have been put forth [13, 14]. The integration of wind power could have an impact on power quality and stability as well. Additionally, the system's capacity for transferring power is reduced by higher and more variable wind penetration [15]. Evaluating the derived voltage stability indices is one method of figuring out the voltage stability of a wind firm. For a specific line loading condition, the voltage stability indices' values would show how far a voltage fall apart would occur [16]. The capability of a power system to preserve constant voltages at all of its buses after being subjected to disturbances of any kind that cause voltage collapse is known as voltage stability [17]. Numerous static voltage stability analysis techniques have been built and advanced over the past few years. The determined analysis methods include V-Q curve, PV curve, the continuation power flow (CPF), and the singularity of the Jacobian matrix based methods. These methods are used to calculate the maximum loading margin, forecast the voltage collapse point, the maximum stability limit, and the point at which the voltage becomes intense. These methods do not consider the deployment of renewable energy resources. The voltage collapse begins at the weakest node of a system and is expressed throughout the network in a very short time span. The problem of voltage collapse must be addressed and hence a number of renewable sources, such as solar PV systems, and wind energy systems are to be integrated to improve the voltage stability. A novel approach is used to analyse the assessment of a constant state probabilistic voltage stability margins (PVSMs), which account both load demand and generating uncertainty [18]. A QV-based method is presented in [19] to evaluate the voltage instability tendencies of power system buses with increasing penetration of RE termed the Critical Voltage-Reactive Power Ratio (CVQR) index. The two-tier load model and distributed generation units (DG) are discussed in [20] along with a modified voltage stability index. To increase voltage stability and lower losses, the Imperialist Competition Algorithm (ICA) is applied to choose the optimal DG size and placement. In the traditional optimal power flow issue for multiobjective optimization (MO), a Voltage Collapse Proximity Index (VCPI) is introduced in the [21] study. A FACTS device called a Distributed Power Flow Controller (DPFC) has been placed in the optimal location along with the optimal size in the system which improves the voltage profile of the system [22]. A study [23] suggests a composite voltage stability index (CVSI) based on the known L-index and the minimal eigenvalue of a reduced Jacobian matrix through which the voltage stability of the system can be minimized. A brand-new line voltage stability index (BVSI) is proposed for identifying weak lines and buses under diverse network designs and loading scenarios [24]. A unique algorithm was developed to enhance the loading margin of the system which trains the machine learning models by producing training data under various operational settings and (N-1) contingencies. When there is a disturbance in the power system, it typically results in instability and can occasionally result in voltage collapse (VC). A cutting-edge method called Vector Analysis (VA) is presented to avoid these issues in [25]. In this study, a new instability detection index is considered for power system large-area voltage stability. The research [26] analyses the Low Voltage Ride-Through (LVRT) characteristics of distributed PV generation before examining the impact of LVRT control techniques and PDG parameters on grid voltage stability. The article [27] explores the difficulties of that future power systems will face related to voltage instability. The interdependence of other infrastructures and future power systems is one of the main issues affecting voltage stability.

To identify the weakest bus, several analysis methods have been developed including voltage stability index, Jacobi matrix singular analysis, sensitivity analysis, eigenvalue analysis [28], as well as P, Q, and V margin indices [29]. Several of these methods necessitate computational investigation, which takes time. The voltage stability indices, on the other hand, has benefits for performance and is appropriate for both dynamic and static assessment. Many line voltage stability indices such as line stability index (Lmn) [30], fast voltage stability index (FVSI) [31], line voltage stability index (LVSI) [32], line stability factor (Lqp) [33], Voltage collapse proximity indicator (VCPI) [34], Thevenins equivalent-based index [35], system voltage recovery index (VRIsys) [36], Novel Line Stability Index (NLSI) [37], power system voltage stability index (PSVSI) [38], and New Global Index [39], etc. have been developed to identify the most severe lines of the electrical networks.

This paper investigates the effects of the integration of wind energy and solar PV generation on static voltage stability. To address the effects, the maximum loading margin of the system and Lmn, FVSI, and Lqp indices have been studied under wide variations in load patterns (50%, 75%, 100%, and 125% system loadings). The proposed algorithm for integrating the RE are being validated in term of voltage stability and loading margin in MATLAB/PSAT software on IEEE 14-bus and IEEE 118-bus systems available online [40].

The numerical outcomes demonstrate the influence of wind energy and PV integration on stability of the power system. The voltage stability of the lines of the system in terms of line stability indices can be improved under all considered load patterns with the integration of the wind and solar PV systems with the test systems. Also, the maximum loadability of the system gets highly increased after integration of the wind and solar PV system with the test systems under 50%, 75%, 100%, and 125% of system loadings. For the study and regulation of electric power systems, PSAT is a Matlab toolbox that is accessible online. PSAT allows for the plotting and analysis of time domain simulation, small signal stability analysis, the power flow (PF), optimal power flow, and continuation power flow (CPF) to track different potential points of collapse within the system. This toolbox also offers a full graphical

user interface and an online network editor that is based on Simulink. The PSAT is a graphical user interfaces (GUIs) software can be used to evaluate all processes efficiently. An accessible toolkit for network design is provided via a Simulink-based library in PSAT. Utilizing PSAT has the benefit of enabling the creation of electrical schemes and multi-machine networks utilizing visual blocks.

The voltage stability of the system can be accessed by the proposed approach very accurately in terms of line stability indices which can avoid the voltage instability situations. After identifying the weak lines of the system, under stressed conditions, weak lines can be removed from the system in order to minimise their impact, concequently, damage will not occur in over- or under-voltage situations. The deployment of RE with the network reduces the line stability indices which shows that the line gets in normal condition from stressed condition. The proposed approach has tested from light loading conditions (50% of system loading) to heavy loading conditions (125% of system loading). Hence the proposed method is able to access the voltage stability under different operating scenarios.

2. ASSESSMENT OF VOLTAGE STABILITY USING LINE VOLTAGE STABILITY INDEX AND CONTINUATION POWER FLOW (CPF)

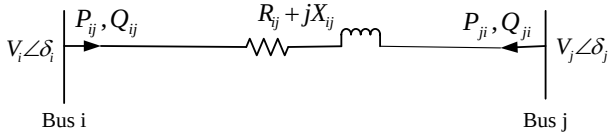

Fig. 1. Two bus power systems.

A simple two-bus power system is represented by Fig. 1. For this system, the voltage stability may be accessed by a number of stability indices, mainly, line stability index (Lmn) [30], fast voltage stability index (FVSI) [31], and line stability factor (Lqp) [33]. These indices may be defined by:

$$Lmn_{ij} = \frac{4X_{ij}Q_{ji}}{(V_i \sin(\theta_{ij} - \delta_{ij}))^2}, \tag{1}$$

$$FVSI_{ij} = \frac{4|Z|^2 Q_{ji}}{V_i X_{ij}}, \tag{2}$$

$$Lqp_{ij} = 4\left(\frac{X_{ij}}{V_i^2}\right)\left(\frac{X_{ij}}{V_i^2}{P_{ij}}^2 + Q_{ji}\right). \tag{3}$$

where X_{ij} is the line reactance, V_i is the sending end voltage, Q_{ji} is the reactive power at the receiving end, is the line impedance angle, Z_{ij} is the line impedance, P_{ij} is the real power flow at the sending end, and δ_{ij} is the power angle. For a stable system, Lmn, FVSI, and Lqp stability indices should be less than unity, otherwise system will become in unstable condition.

2.1. Continuation power flow (CPF) for load flow analysis

A computational tool called CPF analyses how parameter variations affect the voltage stability of power systems [41]. Robustness and fast computational speed in solving faulty power flow solutions near to the nose point are the main advantages of the CPF over other continuation methods. Instead of using conventional power flow equations to solve the numerical problem near the nose point, CPF uses extended nonlinear arithmetical calculations. Step-length control, corrector, parameterization, and predictor are the core components of CPF as shown in Fig. 2.

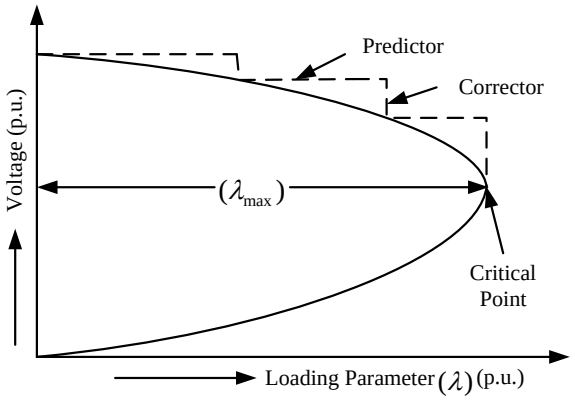

Fig. 2. Nose curve obtained from CPF method.

With reference to Fig. 2, the prediction step computes the digression vector to estimate the next solution for a given load increment pattern. Using the Newton-Raphson load flow method, the corrective phase then modifies this anticipated solution to yield the precise solution [42]. Following this, a new predicted solution based on the new tangent vector is obtained for the subsequent load increment, and a correction step is then performed to obtain the accurate result. Until the voltage collapse significant point is achieved, this process continues. The tangent vector turns to zero at this point. For each load increment, the PV curve is created as a result of the group of corrected solutions.

PV curve analysis is a tried-and-true method for analyzing the voltage stability of a power system. It offers a way to calculate the maximum load factor, a measure of the system's maximum (critical) scalable load demand required for stable grid operation, which can be used to calculate the voltage stability limit. PV curves demonstrate how bus voltages change about the system's loading parameter, indicating how the increase in load is proportionally distributed among the load buses. The PV curve, which is derived from continuous power flow, provides the steady state voltage stability limit as indicated by the turning point of the PV nose curve, which shows the location of the peak load demand and the subsequent critical voltage.

2.2. Algorithm of proposed approach

The voltage stability assessment of the test systems using proposed method can be achieved through the following steps:

Step 1. Run the CPF for base loading and for each load buses obtained the bus voltage magnitude and angle, real and reactive generated, and real as well as reactive power load.

Step 2. Decide the most severe bus of the system based on bus voltage magnitude at the maximum loading point.

Step 3. Place the wind energy system at the most severe bus of the system as decided in Step 2 and by following Step 1 obtain bus voltage magnitude and angle, real and reactive generated, and real as well as reactive power load for each bus.

Step 4. Deploy the solar PV system at the most critical bus of the test system and repeat Step 3.

Step 5. Obtain the line flow data of the test system using the CPF method under 50%, 75%, 100%, and 125% of system loadings for the base case, with wind energy integration, and solar PV generation integration at the most severe bus of the system.

Step 6. Using line flow data obtained in Step 5 in Eq. (1), calculate the Lmn indices of all lines of the system under four types of considered system loading for the base case, with wind energy integration, and with solar PV generation integration at the most severe bus of the system.

Step 7. Using line flow data obtained in Step 5 in Eq. (2), calculate the FVSI indices of all lines of the system under four

types of considered system loading for the base case, with wind energy integration, and with solar PV generation integration at the most severe bus of the system.

Step 8. Using line flow data obtained in Step 5 in Eq. (3), calculate the Lmn indices of all lines of the system under four types of considered system loading for the base case, with wind energy integration, and with solar PV generation integration at the most severe bus of the system.

Step 9. Compare the line indices of top severe lines calculated in Steps 6, 7, and 8 under different considered operating scenarios with RE integration.

Step 10. Obtain the maximum loadability of the system under 50%, 75%, 100%, and 125% of system loadings. Also, compare the maximum loadability evaluated under these operating conditions with and without wind and solar PV generation integration with the system.

All the steps involved in assessing the voltage stability on a test system have been pictorially presented as a flowchart in Fig. 3.

2.3. Integration of wind energy system with power system

Small-scale wind systems found within the distribution system and build of doubly fed induction generators (DFIG) are growing quickly in the current situation [43]. A small signal stability investigation and evaluation of the effects of the squirrel cage induction generator (SCIG) and direct field induction generator (DFIG) on the electric power network was previously carried out on the IEEE 14-bus system with the deployment of the wind energy. According to the model results, fixed-speed wind generators are more dependable and easier to use, but they have a lower energy output than wind turbines. Additionally, it is shown that wind generators with variable speeds and similar ratings can significantly increase the system's stability [44]. In this work, only the DFIG wind system is taken into consideration. Mathematically, the wind turbine model can be written as [45]:

The wind turbine's mechanical output power and torque are expressed as follows:

$$P_t = 0.5 C_p(\lambda, \beta) \rho A V_w^3, \tag{4}$$

$$T_t = P_t \frac{P_t}{w_t}. \tag{5}$$

where A is the turbine's swept area in m^2, C_p is the performance coefficient of the turbine, w_t is the rotor blade's tip speed in rad/s, V_w is the wind speed in m/s, ρ is the blade pitch angle and λ is the tip speed ratio. The following expressions are provided for the performance coefficient (C_p) and tip-speed ratio (λ):

$$C_p(\lambda,\, \beta) = 0.5176 \left(\frac{116}{\lambda_1} - 0.4\beta - 5 \right) e^{\frac{-21}{\lambda_1}} + 0.0068\lambda, \tag{6}$$

$$\lambda_1 = \frac{(\beta^3 + 1)(\lambda + 0.08\beta)}{\beta^3 - 0.028\beta - 0.035\lambda + 1}, \tag{7}$$

$$\lambda = {}^{(w_t R_t)}/_{V_w}. \tag{8}$$

where R_t denotes the turbine blade's radius.

Evaluating the derived voltage stability index is one method of figuring out the voltage stability of a wind-integrated system. For a specific line loading condition, voltage stability index values would show how far it is to voltage instability [46, 47].

2.4. Integration of solar PV generation with power system

Although it has some integration problems, renewable technology improves the voltage stability of the system. Photovoltaic energy integration has gradually increased over the past few years, resulting in a doubling of installation. The goal of modern technology is distributed energy production. The photovoltaic PV module or PV cell should be researched in order to integrate photovoltaic power. PV cells are assembled to form an array. Consequently, a module is the name given to the union of a series and a parallel array [48]. Grid integration of PV systems has significantly increased more recently than ever before as a result of governmental incentives to promote environmentally friendly energy sources and the ongoing development of power electronics-based energy conversion technologies. There are connections between PV systems in distribution networks, sub-transmission networks, and the transmission networks that range in size from hundreds of megawatts (MW) to a few kilowatts (kW). Photovoltaic systems have an efficiency of under 40%. The main drawback of solar energy is that it is dependent on the amount of solar radiation available. Therefore, the AC-DC/DC-AC conversion also contributes to system losses [49, 50].

3. RESULTS AND DISCUSSIONS

The applicability and validity of the proposed method have been tested on two systems namely IEEE 14-bus and IEEE 118-bus systems. The proposed analysis has been validated with renewable energy integration through MATLAB/PSAT software. The most critical line has been found based on calculated Lmn, FVSI, and Lqp values. The maximum loading parameter $\lambda_{\max}$ for both test systems has been assessed using CPF for four types of system loading scenarios (50%, 75%, 100%, and 125%) with and without deployment of the wind or solar energy systems. Under the 50%, 75%, 100%, and 125% system loading scenarios, the active and reactive power of all system load buses are multiplied by the factors of 0.50, 0.75, 1.00, and 1.25, respectively.

3.1. IEEE 14-bus system

To examine the validity and applicability of the proposed approach, the IEEE 14-bus system [40] is considered a test system available in MATLAB/PSAT software. This system consists of 16 lines, 5 generators, 4 transformers, 14 buses, and 11 load buses.

A) Severity of the buses

Newton-Raphson Load Flow (NRLF) can provide the solution at a single operating point. To track the collapse point, NRLF should be run multiple times at different loading. It is difficult to achieve the collapse point using NRLF. Hence a new technique, CPF has been evolved to provide the accurate collapse point using predictor-corrector techniques. The maximum loading parameter for the IEEE 14-bus system has been found as $\lambda_{\max}$ 1.6954 p.u. .at or near the collapse point. For this point, the voltage at bus 14 is 0.7153 p.u. as shown in Table 1 which is the smallest among the all-load bus voltage magnitude. Hence bus number 14 is considered to be the most critical bus at the nose point.

The most stressed bus of the IEEE 14-bus system is found to be the 14^{th} bus using CPF. Hence, at this bus, reactive power support devices such as wind energy and solar PV generation can be connected to enhance the voltage magnitude at bus 14. In this paper, bus number 14 is chosen as the most severe bus and the effect of wind firm and solar PV generation are analyzed after connecting these with bus number 14.

In this paper, the wind farm is placed at bus number 14 and the CPF is run for the IEEE 14-bus system to see the impact of wind integration. With wind integration, the voltage at bus 14 has been enhanced from 0.7153 p.u.. to 0.7191 p.u. With wind integration bus 14 is still the most severe bus of the system as evident from Table 2. In this study, the solar PV system is also located at bus number 14, and the IEEE 14-bus system CPF is run to assess the

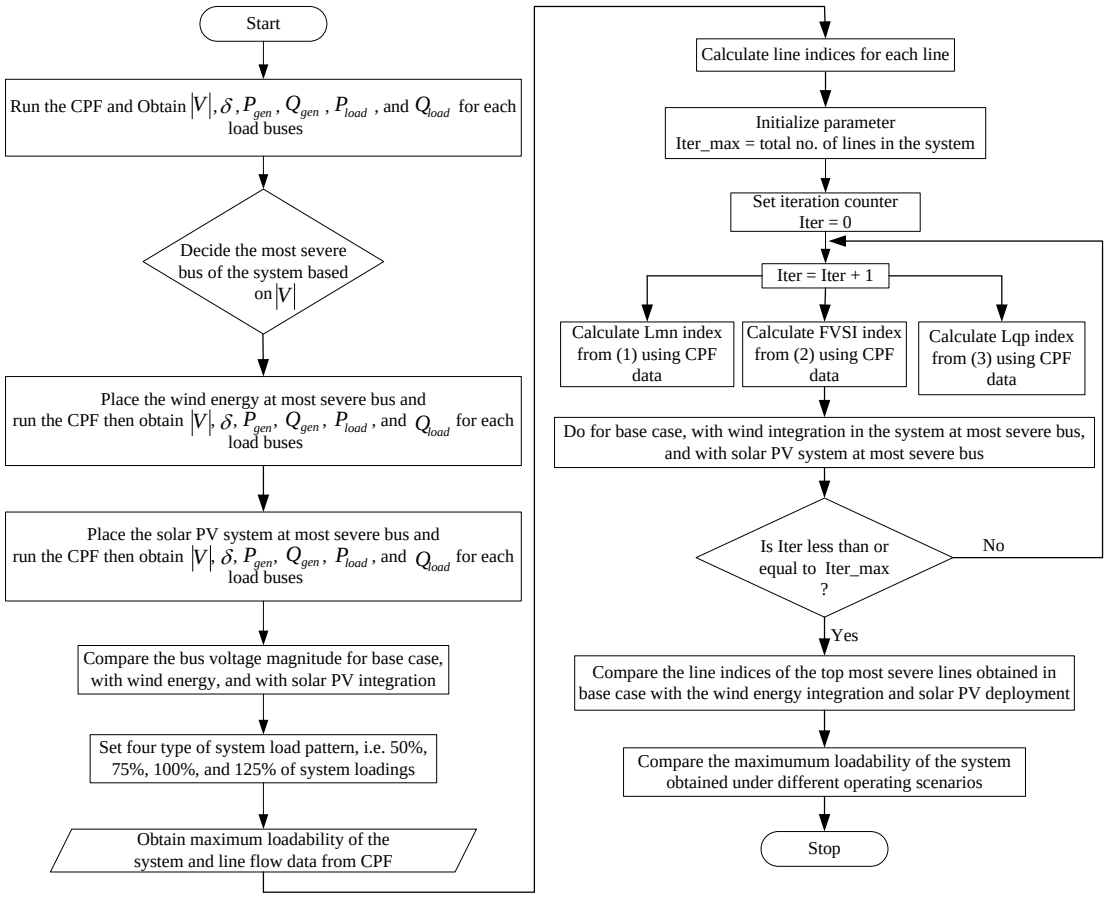

Fig. 3. Flowchart of the proposed algorithm.

Table 1. Base case bus data of IEEE 14-bus system without wind or solar PV integration.

Bus Number	V (p.u.)	Phase (deg)	P_{gen}(p.u.)	Q_{gen}(p.u.)	P_{load}(p.u.)	Q_{load}(p.u.)
1	1.0600	0.0000	7.7641	2.3902	0.0000	0.0000
2	0.9314	-17.9940	-0.1020	1.7701	0.5147	0.3012
3	0.8727	-45.8259	-0.0197	1.6899	2.2343	0.4507
4	0.7991	-35.4217	0.0000	0.0000	1.1338	0.0949
5	0.8118	-29.6151	0.0000	0.0000	0.1803	0.0380
6	0.8625	-51.9349	-0.0179	0.8872	0.2657	0.1779
7	0.8429	-47.4016	0.0000	0.0000	0.0000	0.0000
8	1.0039	-47.5689	-0.0140	0.9179	0.0000	0.0000
9	0.7702	-53.9167	0.0000	0.0000	0.6997	0.3937
10	0.7622	-54.7554	0.0000	0.0000	0.2135	0.1376
11	0.8005	-53.7725	0.0000	0.0000	0.0830	0.0427
12	0.8106	-55.2559	0.0000	0.0000	0.1447	0.0380
13	0.7907	-55.4917	0.0000	0.0000	0.3202	0.1376
14	0.7153	-59.2510	0.0000	0.0000	0.3534	0.1186

Table 2. Base case bus data of IEEE 14-bus system with wind integration.

Bus Number	V (p.u.)	Phase (deg)	P_{gen}(p.u.)	Q_{gen}(p.u.)	P_{load}(p.u.)	Q_{load}(p.u.)
1	1.0600	0.0000	7.7572	2.3536	0.0000	0.0000
2	0.9328	-17.9733	-0.1012	1.7722	0.5148	0.3013
3	0.8753	-45.6767	-0.0197	1.6937	2.2348	0.4508
4	0.8017	-35.3231	0.0000	0.0000	1.1340	0.0949
5	0.8142	-29.5497	0.0000	0.0000	0.1803	0.0380
6	0.8660	-51.7170	-0.0179	0.8902	0.2657	0.1779
7	0.8455	-47.2146	0.0000	0.0000	0.0000	0.0000
8	1.0053	-47.3786	-0.0138	0.9119	0.0000	0.0000
9	0.7734	-53.6778	0.0000	0.0000	0.6999	0.3938
10	0.7655	-54.5099	0.0000	0.0000	0.2135	0.1376
11	0.8040	-53.5371	0.0000	0.0000	0.0830	0.0427
12	0.8144	-55.0102	0.0000	0.0000	0.1447	0.0380
13	0.7944	-55.2428	0.0000	0.0000	0.3203	0.1376
14	0.7191	-58.9639	0.0000	0.0000	0.3535	0.1186

Table 3. Base case bus data of IEEE 14-bus system with solar PV integration.

Bus Number	V (p.u.)	Phase (deg)	P_{gen}(p.u.)	Q_{gen}(p.u.)	P_{load}(p.u.)	Q_{load}(p.u.)
1	1.0600	0.0000	8.6823	3.2960	0.0000	0.0000
2	0.8893	-20.4734	-0.2081	1.7038	0.5822	0.3408
3	0.7843	-55.2403	-0.0212	1.5583	2.5275	0.5098
4	0.7751	-41.2516	0.0000	0.0000	1.2825	0.1073
5	0.7933	-34.3125	0.0000	0.0000	0.2039	0.0429
6	0.9457	-54.6323	-0.0181	0.9572	0.3005	0.2012
7	0.8858	-51.7806	0.0000	0.0000	0.0000	0.0000
8	1.0250	-51.9024	-0.0110	0.8098	0.0000	0.0000
9	0.8583	-56.7820	0.0000	0.0000	0.7915	0.4454
10	0.8490	-57.4951	0.0000	0.0000	0.2415	0.1556
11	0.8853	-56.4700	0.0000	0.0000	0.0939	0.0483
12	0.9171	-57.4461	0.0000	0.0000	0.1637	0.0429
13	0.9208	-57.9992	0.0000	0.0000	0.3622	0.1556
14	0.9970	-60.8220	0.4000	0.8749	0.3998	0.1342

consequences of solar PV integration. The voltage at bus 14 has increased due to wind integration from 0.7153 p.u. to 0.9970 pu. As seen in Table 3, bus 14 is now no longer the most severe bus after the solar PV integration of 40 MW with the system.

B) Line voltage stability indices

Line voltage stability indices can predict the line voltage stability of the system. In this paper, Lmn, FVSI, and Lqp line voltage stability indices are used to find the stability of the lines under 50%, 75%, 100%, and 125% system loadings. Under these operating conditions, the considered line stability indices are also evaluated with and without wind and solar energy integration and compared with each other.

A.1) Lmn indices with and without deployment of wind and solar PV integration

The line indices Lmn, value has been calculated by using CPF

Table 4. Line stability index Lmn for different lines of IEEE 14-bus system at 50% and 75% system loadings.

Lines		Lmn index (in p.u.) at 50% system loading			Lmn index (in p.u.) at 75% system loading		
From Bus	To Bus	Without wind and PV integration	With wind integration	With solar PV integration	Without wind and PV integration	With wind integration	With solar PV integration
2	5	0.1648	0.1631	0.0086	0.3648	0.3533	0.2149
6	12	0.1208	0.1184	0.0158	0.1457	0.1434	0.0261
12	13	0.0724	0.0711	0.0615	0.0818	0.0809	0.0629
6	13	0.2028	0.2021	0.0285	0.2414	0.2377	0.0170
6	11	0.2461	0.2442	0.1743	0.2599	0.2588	0.2167
11	10	0.1796	0.1791	0.1123	0.1797	0.1600	0.1432
9	10	0.0002	0.0001	0.0212	0.0158	0.0142	0.0117
9	14	0.0653	0.0643	0.5260	0.1291	0.1226	0.1166
14	13	0.2238	0.2236	0.4857	0.2347	0.2339	0.2203
7	**9**	**0.3143**	**0.3124**	**0.0874**	0.4165	0.4053	0.1192
1	**2**	**0.5569**	**0.5559**	**0.4396**	0.3848	0.3683	0.3577
5	**1**	**1.0724**	**1.0721**	**0.9881**	**0.9596**	**0.9515**	**0.9473**
3	**2**	**0.9907**	**0.9901**	**0.9294**	**1.0023**	**0.9934**	**0.9233**
3	4	0.1322	0.1312	0.1159	0.0708	0.0696	0.0558
5	4	0.0544	0.0541	0.0537	0.0470	0.0462	0.0364
2	**4**	0.1706	0.1702	0.0306	**0.3986**	**0.3839**	**0.2975**
4	**9**	0.2741	0.2732	0.1481	**0.8806**	**0.8304**	**0.5150**
5	6	0.1091	0.1088	0.0815	0.1972	0.1907	0.0669
4	7	0.1152	0.1146	0.1012	0.0488	0.0481	0.0388
8	**7**	**0.7320**	**0.7315**	**0.5654**	**0.8647**	**0.8433**	**0.6752**

Table 5. Line stability index Lmn for different lines of IEEE 14-bus system at 100% and 125% system loadings.

Lines		Lmn index (in p.u.) at 100% system loading			Lmn index (in p.u.) at 125% system loading		
From Bus	To Bus	Without wind and PV integration	With wind integration	With solar PV integration	Without wind and PV integration	With wind integration	With solar PV integration
2	5	0.4114	0.4048	0.2770	0.4053	0.4011	0.2836
6	12	0.1526	0.1512	0.0349	0.1507	0.1498	0.0503
12	13	0.0842	0.0837	0.0571	0.0831	0.0828	0.0376
6	13	0.2519	0.2498	0.0039	0.2486	0.2472	0.0254
6	11	0.2621	0.2614	0.2220	0.2590	0.2586	0.2269
11	10	0.1783	0.1779	0.1448	0.1762	0.1761	0.1491
9	10	0.0204	0.0196	0.0177	0.0202	0.0196	0.0175
9	14	0.1489	0.1452	0.1302	0.1461	0.1438	0.1290
14	13	0.2366	0.2361	0.2330	0.2340	0.2337	0.2240
7	9	0.4471	0.4408	0.1494	0.4408	0.4368	0.1810
1	2	0.3449	0.3370	0.3274	0.3040	0.2992	0.2866
5	**1**	**0.9255**	**0.9248**	**0.9188**	**0.9163**	**0.9171**	**0.9162**
3	**2**	**1.0000**	**0.9954**	**0.9189**	**0.9806**	**0.9777**	**0.9010**
3	4	0.0400	0.0347	0.0200	0.0409	0.0397	0.0345
5	4	0.0436	0.0431	0.0302	0.0439	0.0434	0.0317
2	**4**	**0.4560**	**0.4476**	**0.3783**	**0.4488**	**0.4434**	**0.3747**
4	**9**	**1.0556**	**1.0256**	**0.3923**	**1.0158**	**0.9970**	**0.2678**
5	6	0.2214	0.2174	0.0498	0.2155	0.2130	0.0234
4	7	0.0357	0.0345	0.0276	0.0400	0.0393	0.0235
8	**7**	**0.9104**	**0.8989**	**0.7271**	**0.9015**	**0.8943**	**0.7353**

Table 6. Line stability index FVSI for different lines of IEEE 14-bus system at 50% and 75% system loadings.

Lines		FVSI index (in p.u.) at 50% system loading			FVSI index (in p.u.) at 75% system loading		
From Bus	To Bus	Without wind and PV integration	With wind integration	With solar PV integration	Without wind and PV integration	With wind integration	With solar PV integration
2	5	0.1784	0.1765	0.0094	0.3978	0.3852	0.2362
6	12	0.1260	0.1252	0.164	0.1531	0.1505	0.0272
12	13	0.0729	0.0725	0.0628	0.0825	0.0816	0.0643
6	13	0.2126	0.2122	0.0299	0.2553	0.2512	0.0179
6	11	0.2520	0.2519	0.1789	0.2673	0.2661	0.2229
11	10	0.1817	0.1817	0.1138	0.1823	0.1815	0.1453
9	10	0.0002	0.0002	0.0001	0.0159	0.0143	0.0219
9	14	0.0694	0.0685	0.0528	0.1390	0.1319	0.1024
14	13	0.2121	0.2120	0.2051	0.2196	0.2192	0.2033
7	**9**	**0.3117**	**0.3105**	**0.0870**	0.4116	0.4007	0.1184
1	**2**	**0.6148**	**0.6118**	**0.4225**	0.4259	0.4077	0.4062
5	**1**	**0.5797**	**0.5793**	**0.6013**	**0.5289**	**0.5225**	**0.5187**
3	**2**	**0.6413**	**0.6412**	**0.5321**	**0.6102**	**0.6094**	**0.4488**
3	4	0.1466	0.1456	0.1380	0.0787	0.0778	0.0713
5	4	0.0572	0.0571	0.0569	0.0495	0.0484	0.0387
2	**4**	0.1886	0.1878	0.0339	**0.4416**	**0.4253**	**0.3294**
4	**9**	0.2558	0.2589	0.5241	**0.7985**	**0.7551**	**0.4813**
5	6	0.0977	0.0969	0.0749	0.1703	0.1654	0.0593
4	7	0.1119	0.1115	0.1104	0.0468	0.0466	0.0285
8	**7**	**0.7320**	**0.7314**	**0.5654**	**0.8647**	**0.8433**	**0.6752**

Table 7. Line stability index FVSI for different lines of IEEE 14-bus system at 100% and 125% system loadings.

Lines		FVSI index (in p.u.) at 100% system loading			FVSI index (in p.u.) at 125% system loading		
From Bus	To Bus	Without wind and PV integration	With wind integration	With solar PV integration	Without wind and PV integration	With wind integration	With solar PV integration
2	5	0.4496	0.4424	0.3050	0.4432	0.4386	0.3121
6	12	0.1607	0.1592	0.0365	0.1586	0.1576	0.0526
12	13	0.0849	0.0844	0.0583	0.0839	0.0836	0.0383
6	13	0.2670	0.2646	0.0042	0.2633	0.2618	0.0268
6	11	0.2699	0.2692	0.2286	0.2666	0.2661	0.2335
11	10	0.1809	0.1807	0.1469	0.1787	0.1787	0.1512
9	10	0.0207	0.0198	0.0197	0.0204	0.0198	0.0149
9	14	0.1609	0.1568	0.1445	0.1577	0.1551	0.1445
14	13	0.2206	0.2203	0.2201	0.2184	0.2183	0.2170
7	9	0.4413	0.4352	0.1482	0.4352	0.4314	0.1476
1	2	0.3819	0.3732	0.3604	0.3366	0.3312	0.3206
5	**1**	**0.5201**	**0.5200**	**0.5176**	**0.5243**	**0.5240**	**0.5197**
3	**2**	**0.5983**	**0.5979**	**0.4326**	**0.5892**	**0.5890**	**0.4428**
3	4	0.0445	0.0437	0.0425	0.0454	0.0447	0.0368
5	4	0.0460	0.0465	0.0321	0.0462	0.0452	0.0337
2	**4**	**0.5054**	**0.4961**	**0.4186**	**0.4974**	**0.4915**	**0.4149**
4	**9**	**0.9494**	**0.9239**	**0.3641**	**0.9156**	**0.8996**	**0.2491**
5	6	0.1894	0.1865	0.0438	0.1851	0.1832	0.0207
4	7	0.0342	0.0341	0.0316	0.0383	0.0378	0.0241
8	**7**	**0.9104**	**0.8989**	**0.7271**	**0.9015**	**0.8943**	**0.7353**

data for all lines under wide variations in load patterns as shown in Table 4 and Table 5. The Lmn indices for all lines are also evaluated with wind energy and solar PV generation integration in the system. The critical lines are decided based on Lmn indices values. The most severe line is that who has an Lmn index value near unity. The lines (5-1), (3-2), (8-7), (1-2), and (7-9) are the top five most severe lines of the system under 50% system loading condition as shown in Table 4.

From this table, it is evident that the value of the Lmn index is reduced in the presence of wind or solar PV integration at different system loadings. The critical lines of the system may change under different operating scenarios. From this table, lines (5-1), (3-2), (8-7), (4-9), and (2-4) are found to be the top five most severe lines based on the Lmn index values at 75% system loading. So, this can be concluded that after increasing the system loading most of the lines get more stress, but some lines may get relaxed. It is observed that from Table 5, after the integration of wind energy and solar PV generation with the system, the line indices values are reduced in both cases (100% and 125% system loadings), but in the case of solar PV generation, the line indices values are highly reduced in comparison to the case of wind energy integration. In the same pattern, from Table 5, it is observed that the lines (5-1), (3-2), (8-7), (4-9), and (2-4) are the top 5 most severe lines under 100% and 125% system loading conditions. From this Table, it is evident when wind or solar PV integration is present at different system loadings, the value of the Lmn index decreases.

From Tables 4 and 5, it is evident that the value of Lmn indices with the wind or solar PV integration at the specified top five critical lines are reduced at different system loadings (50%, 75%, 100%, and 125%).

A.2) FVSI indices with and without deployment of wind and solar PV integration

With the system's integration of wind energy and solar PV generation, the Lmn indices for all lines are assessed. Based on the values of the FVSI indices, the critical lines are selected. The line with an FVSI index value close to unity is the most severe line of the system. From Table 6, the top five most severe lines of the system under a 50% system loading scenario are lines (5-1), (3-2), (8-7), (1-2), and (7-9). This table makes it clear that the value of the FVSI index decreases when wind or solar PV integration is present at various system loadings. The system's severe lines may alter depending on the operating conditions. Based on FVSI index values at 75% system loading, lines (5-1), (3-2), (8-7), (4-9), and (2-4) are identified as the top five most severe lines in this table. Therefore, it may be argued that as system loading is increased, most lines experience increased stress while some lines may experience relief.

It can be seen from Table 7 that the line indices values are reduced in both cases (100% and 125% system loadings) after the integration of wind energy and solar PV generation with the systems, but they are significantly reduced in the case of solar PV generation compared to the case of wind energy integration. The lines (5-1), (3-2), (8-7), (4-9), and (2-4) are the top 5 most severe lines at 100% and 125% system loading situations, as seen in Table 7. This Table shows that the value of the FVSI index drops when wind or solar PV integration is present in the system at different system loadings.

It is evident from Tables 6 and 7 that at different system loadings (50%, 75%, 100%, and 125%), the value of FVSI indices with the integration of wind or solar PV is reduced at the stipulated top five severe lines.

Table 8. Line stability index Lqp for different lines of IEEE 14-bus system at 50% and 75% system loadings.

Lines		Lqp index (in p.u.) at 50% system loading			Lqp index (in p.u.) at 75% system loading		
From Bus	To Bus	Without wind and PV integration	With wind integration	With solar PV integration	Without wind and PV integration	With wind integration	With solar PV integration
2	5	0.2949	0.2941	0.1410	0.5724	0.5560	0.4641
6	12	0.1162	0.1154	0.0204	0.1446	0.1419	0.0321
12	13	0.0334	0.0334	0.0282	0.0379	0.0375	0.0289
6	13	0.1891	0.1885	0.0153	0.2323	0.2221	0.0020
6	11	0.2152	0.2143	0.1538	0.2305	0.2292	0.1926
11	10	0.1574	0.1573	0.0990	0.1585	0.1585	0.1266
9	10	0.0007	0.0006	0.0005	0.0149	0.0135	0.0199
9	14	0.0816	0.0822	0.0522	0.1561	0.1485	0.1432
14	13	0.1503	0.1502	0.1448	0.1491	0.1496	0.3979
7	9	0.3486	0.3478	0.1059	0.4675	0.4547	0.1471
1	2	0.3670	0.3664	0.3591	0.2811	0.2720	0.2346
5	**1**	**1.0083**	**1.0080**	**1.0048**	**1.0836**	**1.0816**	**1.0094**
3	**2**	**0.6801**	**0.6798**	**0.6537**	0.6420	0.6405	0.5777
3	**4**	**0.8512**	**0.8506**	**0.7942**	**0.9185**	**0.8850**	**0.8175**
5	4	0.0188	0.0186	0.0086	0.0082	0.0079	0.0065
2	**4**	**0.4740**	**0.4731**	**0.3519**	**0.8400**	**0.8141**	**0.8092**
4	**9**	**2.1065**	**2.1051**	**0.9696**	**2.9960**	**2.9091**	**1.8529**
5	6	0.1349	0.1343	0.0524	0.2253	0.2187	0.0281
4	7	0.0054	0.0053	0.0044	0.1032	0.0983	0.0709
8	**7**	**0.7321**	**0.7315**	**0.5654**	**0.8647**	**0.8433**	**0.6752**

Table 9. Line stability index Lqp for different lines of IEEE 14-bus system at 100% and 125% system loadings.

Lines		Lqp index (in p.u.) at 100% system loading			Lqp index (in p.u.) at 125% system loading		
From Bus	To Bus	Without wind and PV integration	With wind integration	With solar PV integration	Without wind and PV integration	With wind integration	With solar PV integration
2	5	0.6468	0.6374	0.5635	0.6447	0.6387	0.5627
6	12	0.1526	0.1510	0.0408	0.1504	0.1494	0.0543
12	13	0.0391	0.0388	0.0262	0.0386	0.0384	0.0172
6	13	0.2444	0.2419	0.0102	0.2407	0.2392	0.0350
6	11	0.2332	0.2325	0.1979	0.2302	0.2298	0.2018
11	10	0.1574	0.1574	0.1282	0.1554	0.1551	0.1316
9	10	0.0198	0.0184	0.0233	0.0189	0.0184	0.0127
9	14	0.1799	0.1755	0.1726	0.1761	0.1733	0.1518
14	13	0.1480	0.1478	0.1371	0.1470	0.1466	0.1395
7	9	0.5030	0.4958	0.1806	0.4955	0.4910	0.2125
1	2	0.2588	0.2542	0.2451	0.2348	0.2319	0.2287
5	**1**	**1.1113**	**1.0124**	**1.0057**	**1.1303**	**1.1301**	**1.0525**
3	2	0.6282	0.6274	0.5568	0.6175	0.6170	0.5527
3	**4**	**0.9256**	**0.9085**	**0.8664**	**0.8707**	**0.8602**	**1.4002**
5	4	0.0046	0.0045	0.0035	0.0062	0.0061	0.0055
2	**4**	**0.9408**	**0.9261**	**0.9120**	**0.9327**	**0.9233**	**0.9134**
4	**9**	**3.2135**	**3.1664**	**2.1672**	**3.1320**	**3.1023**	**2.1424**
5	6	0.2497	0.2457	0.0091	0.2443	0.2418	0.0143
4	7	0.1278	0.1247	0.1197	0.1201	0.1181	0.1177
8	**7**	**0.9104**	**0.8990**	**0.7272**	**0.9016**	**0.8944**	**0.7353**

A.3) Lqp indices with and without deployment of wind and solar PV integration

The Lqp indices values are calculated under the same scenarios also. The lines (5-1), (3-2), (8-7), (4-9), and (3-4) have the highest Lqp indices under 50% system loading as shown in Table 8. So these lines are the top five severe lines of the system. But under 75% system loading, the severity of all lines gets increased due to an increase in Lqp indices values. Under this situation, the lines (5-1), (2-4), (8-7), (4-9), and (3-4) are the top severe lines of the system. From Table 8, The value of these critical lines gets improved after connecting the wind energy and solar PV generation with the system under 50% and 75% system loading conditions.

Whenever the system loading increases up to 100% and 125% the Lqp line indices values of the lines (5-1), (2-4), (8-7), (4-9), and (3-4) get highly near to the unity as shown in Table 9. So these lines are the top five most severe lines of the system. After connecting the wind energy and solar PV generation with the system under 100% and 125% system loading conditions, the value of these critical lines improves as shown in Table 9.

C) Maximum loadability of the system

The maximum loadability ($\lambda_{\max}$) of the system under different operating scenarios is shown in Table 10. The maximum loadability of the system at 50%, 75%, 100%, and 125% system loadings are 3.0514 p.u., 2.2133 p.u., 1.6954 p.u., and 1.3708 p.u., respectively without integration of the wind or solar PV generation in the system. As the system loading increases, the $\lambda_{\max}$ of the system gets reduced. After connecting the wind firm with bus number 14, the maximum loadability of the system becomes 3.0516 p.u., 2.2136 p.u., 1.6956 p.u., and 1.3709 p.u. at 50%, 75%, 100%, and 125% system loadings, respectively. After connecting the solar PV generation with bus number 14, the maximum loadability of the system becomes 3.3683 p.u., 2.5003 p.u., 1.918 p.u., and 1.5466 p.u.at these system loadings as shown in Table 10 and Fig 4.

Table 10. System loadability of IEEE 14-bus system under different system loadings.

Maximum system loadability	At 50% system loading			At 75% system loading		
	Without wind and PV integration	With wind integration	With solar PV integration	Without wind and PV integration	With wind integration	With solar PV integration
$\lambda_{\max}$ (p.u)	3.0514	3.0516	3.3683	2.2133	2.2136	2.5003
Maximum system loadability	**At 50% system loading**			**At 75% system loading**		
	Without wind and PV integration	With wind integration	With solar PV integration	Without wind and PV integration	With wind integration	With solar PV integration
$\lambda_{\max}$ **(p.u)**	1.6954	1.6956	1.918	1.3708	1.3709	1.5466

Table 11. Top five critical lines under 50% and 75% system loadings.

At 50% system loading				At 75% system loading			
Critical lines	Lmn index	FVSI index	Lqp index	Critical lines	Lmn index	FVSI index	Lqp index
5-1	1.0724	0.5797	1.0083	3-2	1.0023	0.6102	0.642
3-2	0.9907	0.6413	0.6801	5-1	0.9596	0.5289	1.0836
8-7	0.732	0.732	0.7321	4-9	0.8806	0.7985	2.996
1-2	0.5569	0.6148	0.367	8-7	0.8647	0.8646	0.8647
7-9	0.3143	0.3117	0.3486	2-4	0.3986	0.4416	0.84
4-9	0.2741	0.2558	2.1065	-	-	-	-
2-4	0.1706	0.1886	0.4740	-	-	-	-

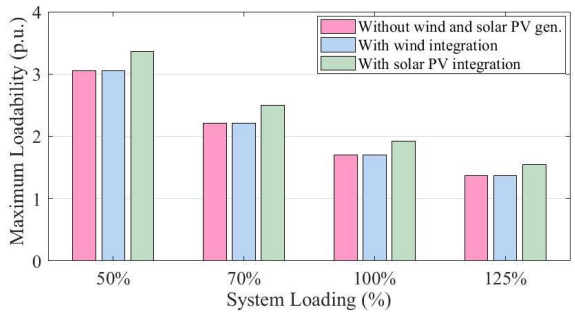

Fig. 4. Bar graph of maximum loadability of IEEE 14-bus system under different operating scenarios.

D) Critical lines under different system loading conditions

The Lmn, FVSI, and Lqp line indices values of the lines (5-1), (3-2), (8-7), (7-9), and (1-2) are very high and highly near to the unity at 50% loading of the system as summarised from Tables 4, 6, and 8. So, these lines are the most severe lines of the IEEE 14-bus system under 50% system loading as shown in Table 11. As the system loading decreases up to 75% the lines (5-1), (3-2), (8-7), (4-9), and (2-4) come under the top five severe most lines as summarised from Tables 4, 6, and 8.

At 100% system loading, the Lmn, FVSI, and Lqp line indices values of the lines (5-1), (3-2), (8-7), (4-9), and (2-4) are extremely high and extremely close to unity as shown in Tables

3.2. IEEE 118-bus system

To demonstrate its applicability to large systems, the suggested method is further evaluated on the IEEE-118 bus system available at [40]. This system consists of 9 transformers, 53 generators, 177 lines, 89 load buses, and 118 buses in the system.

Table 12. Top five critical lines of IEEE 14-bus system under 100% and 125% system loadings.

At 100% system loading				At 125% system loading			
Critical lines	Lmn index	FVSI index	Lqp index	Critical lines	Lmn index	FVSI index	Lqp index
4-9	1.0556	0.9494	3.2135	3-2	1.0158	0.589	0.617
3-2	1	0.5983	0.6282	5-1	0.9806	0.524	1.1301
5-1	0.9255	0.5201	1.1113	4-9	0.9163	0.8996	3.1023
8-7	0.9104	0.9104	0.9104	8-7	0.9015	0.8943	0.8944
2-4	0.4560	0.5054	0.9408	2-4	0.4488	0.4915	0.9233

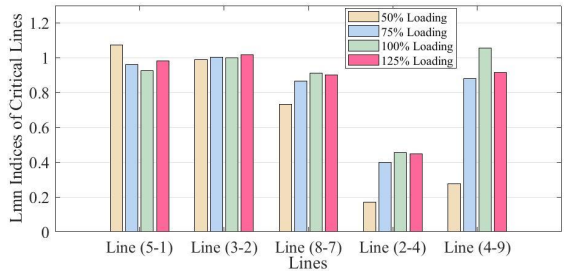

Fig. 5. Bar graph of Lmn indices of most severe lines of IEEE 14-bus system under different system loadings.

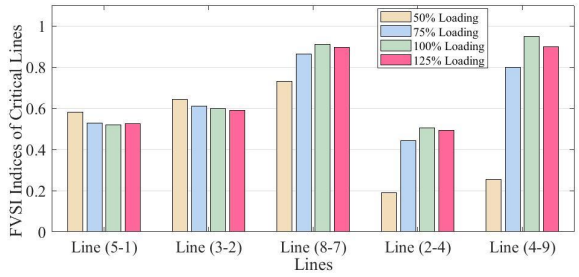

Fig. 6. Bar graph of FVSI indices of most severe lines of IEEE 14-bus system under different system loadings.

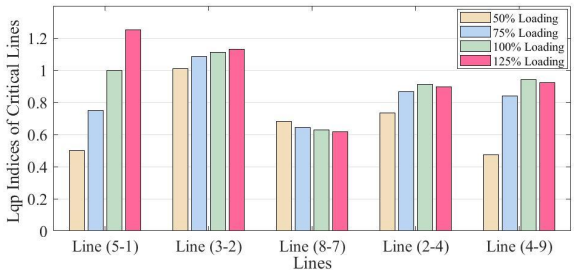

Fig. 7. Bar graph of Lqp indices of most severe lines of IEEE 14-bus system under different system loadings.

A) Severity of the buses

The data on the load flow at a single operating point can be provided by the load flow analysis utilizing the Newton-Raphson method. CPF, on the other hand, can provide the load flow solution when the system is loaded up to the nose point. Table 13 displays the bus voltage magnitudes of twenty lines having the lowest magnitude obtained from the CPF solution for the IEEE 118-bus system's base case, with wind energy integration, with solar PV generation integration in the system. The bus voltage magnitude of bus number 22 is 0.6357 p.u. at maximum loading conditions for the base case, which is the lowest of all the all-load bus voltage magnitudes. Therefore, bus number 22 can be determined as the system's most severe bus when the system is loaded at its maximum loading condition (at the nose point). So, for the IEEE 118-bus system, renewable energy sources or FACTS devices can be placed at bus number 22 to improve the stability of the system. From Table 13, it can be also observed that the bus voltage magnitude of severe most five buses gets reduced after integration of the wind or solar energy systems.

B) Line voltage stability indices

Line voltage stability indices can forecast the system's line voltage stability. The stability of the lines of the IEEE 118-bus system is also determined in this study using the Lmn, FVSI, and Lqp line voltage stability indices.

Table 13. Base case bus data, with wind energy, and solar PV integration for IEEE 118-bus system.

Bus	Base Case		With wind energy		With Solar PV	
Number	V (p.u.)	Phase (deg)	V (p.u.)	Phase (deg)	V (p.u.)	Phase (deg)
22	**0.6357**	**-112.1155**	**0.6358**	**-112.5117**	**0.9690**	**-104.2623**
44	0.6384	-111.6723	0.6386	-111.9819	0.6389	-114.8851
21	0.6497	-132.6088	0.6486	-133.0733	0.8695	-120.5744
45	0.7033	-95.6932	0.7040	-95.9014	0.6927	-98.8345
38	0.7271	-116.5864	0.7275	-117.0549	0.7275	-116.8294

Table 14. Line stability index Lmn for different lines of IEEE 118-bus system at 50% and 75% system loadings.

Lines		Lmn index (in p.u.) at 50% system loading			Lmn index (in p.u.) at 75% system loading		
From Bus	To Bus	Without wind and PV integration	With wind integration	With solar PV integration	Without wind and PV integration	With wind integration	With solar PV integration
44	43	0.1317	0.1315	0.1157	0.5762	0.5761	0.5030
65	**66**	**0.6215**	**0.6213**	**0.5690**	0.7890	0.7888	0.5879
70	**69**	**0.9812**	**0.9811**	**0.2720**	**0.9893**	**0.9891**	**0.0918**
38	37	0.2170	0.2170	0.0251	0.5087	0.5083	0.4759
9	**8**	0.3790	0.3789	0.3038	**0.8493**	**0.8491**	**0.5278**
43	34	0.1527	1526	0.1413	0.5359	0.5359	0.4972
20	19	0.2173	0.2173	0.0578	0.5899	0.5897	0.2895
70	**24**	**0.9603**	**0.9603**	**0.8691**	**0.9615**	**0.9615**	**0.2673**
75	69	0.4791	0.4791	0.4026	0.4958	0.4957	0.2096
75	70	0.0686	0.0684	0.0447	0.1767	0.1761	0.1406
21	20	0.1517	0.1517	0.0207	0.4070	0.4055	0.1506
66	**62**	**0.7271**	**0.7271**	**0.7210**	**0.8176**	**0.8173**	**0.8106**
47	46	0.0958	0.0955	0.0890	0.1278	0.1277	0.1173
30	17	0.4145	0.4141	0.3937	0.6960	0.6960	0.6578
68	**69**	**0.9612**	**0.9601**	**0.9350**	**0.9708**	**0.9708**	**0.1369**
74	70	0.0492	0.0492	0.0390	0.1278	0.1275	0.1012
22	21	0.1067	0.1061	0.0458	0.2576	0.2572	0.0218
59	56	0.1377	0.1376	0.1325	0.5068	0.5063	0.5037
59	56	0.1286	0.1281	0.1235	0.4898	0.4894	0.4867
46	45	0.2551	0.2549	0.2531	0.4306	0.4305	0.4229

B.1) Lmn indices with and without deployment of wind and solar PV integration

Using CPF data for all lines with widely varying load patterns, as illustrated in Tables 14 and 15, the line indices Lmn value has been determined. In these tables, only the Lmn index value of twenty severe most lines are shown. With the system's integration of wind energy and solar PV generation, the Lmn indices for all lines are also assessed. Based on the values of the Lmn indices, the critical lines can be decided. It is observed that the line stability index Lmn of the line gets increased as the system loading increases from 50% to 125%. The Lmn index of the lines gets reduced after the integration of wind energy and solar PV generation under different loading scenarios as shown in Tables 14 and 15. Line numbers (65-66), (70-69), (70-24), (66-62), and (68-69) are found as the top five severe lines under 50% system loading. Whereas these are also under five severe most for 75% system loading except line (65-66). In this situation line (9-8) comes under five severe lines. Lines (44-43), (70-69), (70-24), (38-37), and (68-69) are the five severe lines under both 100% and 125% system loading conditions.

B.2) FVSI indices with and without deployment of wind and solar PV integration

The FVSI Indices are presented in Tables 16 and 17 of the

Table 15. Line stability index Lmn for different lines of IEEE 118-bus system at 100% and 125% system loadings.

Lines		Lmn index (in p.u.) at 100% system loading			Lmn index (in p.u.) at 125% system loading		
From Bus	To Bus	Without wind and PV integration	With wind integration	With solar PV integration	Without wind and PV integration	With wind integration	With solar PV integration
44	**43**	**1.0932**	**1.0931**	**0.5092**	**1.3062**	**1.3058**	**0.9891**
65	66	0.8885	0.8883	0.8152	0.9587	0.9585	0.8438
70	**69**	**1.0124**	**1.0122**	**0.7464**	**1.0795**	**1.0794**	**0.8339**
38	**37**	**0.9872**	**0.9870**	**0.8958**	**1.1131**	**1.1131**	**0.8477**
9	8	0.8546	0.8546	0.5509	0.8925	0.8921	0.4390
43	34	0.5689	0.5682	0.5548	0.9048	0.9048	0.8302
20	19	0.5887	0.5883	0.4653	0.8585	0.8585	0.5790
70	**24**	**0.9825**	**0.9825**	**0.3627**	**0.9830**	**0.9827**	**0.6569**
75	69	0.6663	0.6663	0.5824	0.7011	0.7010	0.6390
75	70	0.3926	0.3925	0.3045	0.4047	0.4043	0.3794
21	20	0.5171	0.5168	0.3706	0.6002	0.6001	0.2960
66	62	0.8674	0.8672	0.1561	0.8957	0.8956	0.3810
47	46	0.1494	0.1493	0.1147	0.7758	0.7758	0.5507
30	17	0.7583	0.7580	0.5194	0.8030	0.8029	0.3934
68	**69**	**1.0517**	**1.0515**	**0.7764**	**1.0825**	**1.0822**	**0.7472**
74	70	0.9321	0.9318	0.9193	0.9599	0.9599	0.8663
22	21	0.8784	0.8784	0.0131	0.8955	0.8954	0.0261
59	56	0.8721	0.8721	0.3714	0.8857	0.88575	0.7081
59	56	0.8468	0.8466	0.7438	0.8667	0.8665	0.6866
46	45	0.7014	0.7014	0.6216	0.8113	0.8110	0.5134

Table 16. Line stability index FVSI for different lines of IEEE 118-bus system at 50% and 75% system loadings.

Lines		FVSI index (in p.u.) at 50% system loading			FVSI index (in p.u.) at 75% system loading		
From Bus	To Bus	Without wind and PV integration	With wind integration	With solar PV integration	Without wind and PV integration	With wind integration	With solar PV integration
44	43	0.1323	0.1321	0.1154	0.5183	0.5182	0.4612
65	66	0.5894	0.5892	0.5571	0.5992	0.6091	0.5918
70	69	0.7548	0.7548	0.2812	0.8771	0.8769	0.0956
38	37	0.2086	0.2081	0.0242	0.4649	0.4647	0.4364
9	8	0.3610	0.3605	0.1607	0.6811	0.6811	2.5808
43	34	0.1480	0.1477	0.1364	0.5389	0.5388	0.5027
20	19	0.2136	0.2135	0.0581	0.5803	0.5803	0.2755
70	24	0.9190	0.9190	0.8290	0.9210	0.9208	0.2662
75	69	0.5307	0.5305	0.5302	0.6112	0.6112	0.2241
75	70	0.0654	0.0651	0.0420	0.1756	0.1756	0.1416
21	20	0.1523	0.1522	0.0210	0.3863	0.3861	0.1402
66	62	0.7514	0.7511	0.7503	0.7605	0.7608	0.7733
47	46	0.0941	0.0941	0.0941	0.1194	0.1189	0.1100
30	17	0.3888	0.3888	0.3715	0.6191	0.6188	0.5904
68	69	0.6809	0.6805	0.6690	0.7406	0.7405	0.1365
74	70	0.0506	0.0501	0.0404	0.1272	0.1271	0.1018
22	21	0.1045	0.1039	0.0442	0.2305	0.2305	0.0195
59	56	0.1193	0.1189	0.1151	0.3783	0.3779	0.3764
59	56	0.1117	0.1116	0.1075	0.3674	0.3670	0.3655
46	45	0.2483	0.2482	0.2470	0.3866	0.3863	0.3819

Table 17. Line stability index FVSI for different lines of IEEE 118-bus system at 100% and 125% system loadings.

Lines		FVSI index (in p.u.) at 100% system loading			FVSI index (in p.u.) at 125% system loading		
From Bus	To Bus	Without wind and PV integration	With wind integration	With solar PV integration	Without wind and PV integration	With wind integration	With solar PV integration
44	**43**	**0.9408**	**0.9406**	**0.9048**	**0.9929**	**0.9927**	**0.9049**
65	66	0.7528	0.7527	0.6588	0.7909	0.7909	0.7072
70	**69**	**0.8978**	**0.8977**	**0.3929**	**0.9649**	**0.9648**	**0.4325**
38	**37**	**0.9080**	**0.9080**	**0.3292**	**0.9314**	**0.9312**	**0.3633**
9	8	0.5721	0.5721	0.5084	0.6290	0.6285	0.5689
43	34	0.5941	0.5940	0.5158	0.8732	0.8727	0.8107
20	19	0.6371	0.6369	0.6098	0.8230	0.8228	0.6275
70	**24**	**0.9215**	**0.9211**	**0.3184**	**0.9383**	**0.9382**	**0.5856**
75	69	0.2544	0.2541	0.1659	0.0310	0.0310	0.0191
75	70	0.1920	0.1918	0.1553	0.4101	0.4101	0.2920
21	20	0.4457	0.4453	0.3188	0.5509	0.5505	0.2638
66	62	0.7691	0.7690	0.5681	0.8534	0.8531	0.5883
47	46	0.2093	0.2091	0.1370	0.4311	0.4307	0.1916
30	17	0.6333	0.6333	0.5796	0.7009	0.7002	0.6804
68	**69**	**0.7902**	**0.7900**	**0.5878**	**0.8963**	**0.8962**	**0.4515**
74	70	0.2103	0.2100	0.1232	0.3353	0.3353	0.2482
22	21	0.3516	0.3511	0.0106	0.3631	0.3630	0.0220
59	56	0.5762	0.5758	0.4230	0.5853	0.5851	0.4929
59	56	0.5632	0.5629	0.4094	0.5753	0.5751	0.4807
46	45	0.5706	0.5701	0.4035	0.8373	0.8371	0.788

top twenty severe lines of IEEE 118-bus system under 50%, 75%, 100%, and 125% system loading conditions. From these tables, it is observed that the FVSI indices of the lines increase as the system loading increases. Following the integration of wind energy and solar PV generation under various loading situations, as illustrated in Tables 16 and 17, the FVSI index of the lines decreases. From Tables 16 and 17, the top five lines with the highest severity under 50% system loading are lines (6566), (7069), (7024), (6662), and (6869). However, except for lines (6566), these are also under five severe for 75% system loading. In this instance, line (9-8) falls under the five most severe lines. Under 100% and 125% system loading conditions, the five most severe lines are lines (44-43), (70-69), (70-24), (38-37), and (68-69).

B.3) Lqp indices with and without deployment of wind and solar PV integration

Tables 18 and 19 show the Lqp Indices for the top 20 most severe lines of the IEEE 118-bus system at 50%, 75%, 100%, and 125% system loading. These tables show that when the system loading grows, the Lqp indices of the lines increase. The Lqp index of the lines falls as wind energy and solar PV power are deployed under various loading conditions, as shown in Tables 18 and 19. In these tables, it is observed that the top five most severe lines with 50% system loading are lines (65-66), (70-69), (70-24), (66-62), and (68-69). While all of these, except lines (65-66), are under five severe for 75% system loading. Line (9-8) falls under the five most severe lines in this loading. The five most severe lines at 100% and 125% system loading are lines (44-43), (70-69), (70-24), (38-37), and (68-69).

C) Maximum loadability of the system

Table 20 displays the system's maximum loadability under various operating conditions. The system's maximum loadability is 4.1303 p.u, 4.1281 p.u., 3.5409 p.u., and 2.4264 p.u. at 50%, 75%, 100%, and 125% system loadings without deployment of the

Table 18. Line stability index Lqp for different lines of IEEE 118-bus system at 50% and 75% system loadings.

Lines		Lqp index (in p.u.) at 50% system loading			Lqp index (in p.u.) at 75% system loading		
From Bus	To Bus	Without wind and PV integration	With wind integration	With solar PV integration	Without wind and PV integration	With wind integration	With solar PV integration
44	43	0.1246	0.1246	0.1084	0.3129	0.3127	0.2758
65	**66**	**0.5796**	**0.5794**	**0.5489**	0.7066	0.7065	0.1171
70	**69**	**0.5680**	**0.5670**	**0.5427**	**0.9012**	**0.9011**	**0.4431**
38	37	0.1286	0.1285	0.1169	0.2885	0.2880	0.0417
9	**8**	0.2676	0.2671	0.105	**0.9627**	**0.9626**	**0.5786**
43	34	0.1241	0.1234	0.1097	0.3726	0.3725	0.2627
20	19	0.1960	0.1956	0.0553	0.4019	0.4011	0.2341
70	**24**	**0.9552**	**0.9547**	**0.3666**	**0.9566**	**0.9562**	**0.7620**
75	69	0.3399	0.3397	0.3246	0.4198	0.4194	0.1118
75	70	0.0395	0.0395	0.0080	0.1614	0.1613	0.1276
21	20	0.1455	0.1453	0.0140	0.2613	0.2611	0.0752
66	**62**	**0.7743**	**0.7739**	**0.4579**	**0.8217**	**0.8216**	**0.5536**
47	46	0.0818	0.0816	0.0811	0.0910	0.0910	0.0718
30	17	0.1506	0.1501	0.1225	0.3311	0.3308	0.0334
68	**69**	**0.8202**	**0.8200**	**0.8941**	**0.8486**	**0.8485**	**0.1510**
74	70	0.0334	0.0331	0.0159	0.1234	0.1231	0.0921
22	21	0.0936	0.0936	0.0790	0.0981	0.0980	0.0397
59	56	0.0084	0.0081	0.0380	0.1619	0.1617	0.0529
59	56	0.0015	0.0012	0.0399	0.1686	0.1683	0.0430
46	45	0.2417	0.2416	0.2130	0.2765	0.2761	0.2188

Table 19. Line stability index Lqp for different lines of IEEE 118-bus system at 100% and 125% system loadings.

Lines		Lqp index (in p.u.) at 50% system loading			Lqp index (in p.u.) at 75% system loading		
From Bus	To Bus	Without wind and PV integration	With wind integration	With solar PV integration	Without wind and PV integration	With wind integration	With solar PV integration
44	**43**	**0.9936**	**0.9935**	**0.9121**	**0.9982**	**0.9980**	**0.4121**
65	66	0.9262	0.9261	0.7705	0.9686	0.9684	0.543
70	**69**	**0.9681**	**0.9680**	**0.6527**	**0.9795**	**0.9793**	**0.7482**
38	**37**	**0.9534**	**0.9531**	**0.4628**	**0.9865**	**0.9861**	**0.7907**
9	8	0.7334	0.7331	0.0148	0.8019	0.8015	0.0978
43	34	0.4273	0.4268	0.3292	0.8197	0.8195	0.7641
20	19	0.5698	0.5696	0.5215	0.7728	0.7726	0.4181
70	**24**	**0.9738**	**0.9737**	**0.9141**	**1.0168**	**1.0161**	**0.3149**
75	69	0.9267	0.9266	0.8221	0.9387	0.9382	0.8447
75	70	0.8555	0.8555	0.7162	0.9758	0.9756	0.7605
21	20	0.8801	0.8800	0.1172	0.9531	0.9527	0.1270
66	62	0.9326	0.9323	0.3441	0.9533	0.9532	0.3636
47	46	0.5988	0.5986	0.3392	0.9739	0.9737	0.9251
30	17	0.3552	0.3550	0.1085	0.4935	0.4932	0.0280
68	**69**	**0.9877**	**0.9877**	**0.5885**	**0.9951**	**0.9948**	**0.5962**
74	70	0.6529	0.6527	0.4751	0.8909	0.8909	0.4767
22	21	0.1307	0.1305	0.1005	0.1910	0.1908	0.1850
59	56	0.3075	0.3073	0.0486	0.4556	0.4554	0.0554
59	56	0.3181	0.3178	0.0363	0.4479	0.4476	0.0443
46	45	0.4867	0.4865	0.4480	0.5951	0.5948	0.2657

Table 20. System loadability of IEEE 118-bus system under different system loadings.

Maximum system loadability	At 50% system loading			At 75% system loading		
	Without wind and PV integration	With wind integration	With solar PV integration	Without wind and PV integration	With wind integration	With solar PV integration
λ_{max} (p.u)	4.1303	4.1475	4.1499	4.1281	4.1425	4.1479
Maximum system loadability	**At 100% system loading**			**At 125% system loading**		
	Without wind and PV integration	With wind integration	With solar PV integration	Without wind and PV integration	With wind integration	With solar PV integration
λ_{max} **(p.u)**	3.5409	3.541	3.6788	2.4264	2.4266	2.5057

Table 21. Comparison of bus voltage magnitude with and without deployment of wind and solar PV system for IEEE 14-bus system.

Bus No.	Bus voltage magnitude (in p.u.) in base case loading				
	Without the integration of wind energy and solar PV system		With wind energy		With Solar PV generator
	Found in [51]	Proposed method	Found in [51]	Proposed Method	Proposed Method
1	1.060	1.060	1.062	1.063	1.063
2	0.931	0.932	1.045	1.046	1.046
3	0.872	0.873	1.014	1.015	1.016
4	0.799	0.799	0.997	0.998	0.999
5	0.811	0.812	1.002	1.003	1.004
6	0.862	0.863	1.074	1.076	1.077
7	0.842	0.843	1.036	1.036	1.037
8	1.003	1.004	1.093	1.094	1.095
9	0.770	0.770	1.012	1.013	1.014
10	0.764	0.762	1.012	1.012	1.012
11	0.800	0.801	1.035	1.036	1.037
12	0.810	0.811	1.046	1.047	1.047
13	0.790	0.791	1.036	1.037	1.038
14	0.715	0.715	0.996	0.997	0.998

RE in the system, respectively. The maximum loadability of the system decreases as system loading rises. The system's maximum loadability increases to 4.1475 p.u., 4.1425 p.u., 3.541 p.u., and 2.4266 p.u. at 50%, 75%, 100%, and 125% system loadings, respectively, once the wind energy is connected to bus number 14. The maximum loadability of the system increases to 4.1499 p.u., 4.1479 p.u., 3.6788 p.u., and 2.5057 p.u. at these system loadings once the solar PV generation is connected to bus number 14, as indicated in Table 20 and Fig 6.

4. COMPARISON OF RESULTS WITH EXISTING RESEARCH

It has been already discussed in section 3.11 Section that the most severe bus of the IEEE 14-bus system (bus number 14) evaluated in this paper is the same as found in [52]. The superiority of the proposed approach to investigate voltage stability can be easily understood by observing Table 21. From Table 21, it is observed that the bus voltage magnitude of the IEEE 14-bus system is highly improved than [51] with wind energy integration in the system. Further after the integration of the solar PV system in the system, the voltage profile of most of the buses gets more improved. So, this can be concluded that, the proposed approach is superior to the existing works.

5. CONCLUSION AND FUTURE WORK

This paper presents a thorough investigation of the voltage stability analysis for the IEEE-14 bus system and IEEE 118-bus system under four types (50% 75%, 100%, and 125%) of system loading conditions. Using CPF, the maximum loading of the system with the base case is being observed near the nose point. At this nose point, the bus with the least value of the voltage magnitude is considered to be the most critical bus and is a suitable location for the deployment of RE. This paper presents a thorough investigation of the voltage stability analysis for the IEEE-14 bus system and IEEE 118-bus system under four types (50% 75%, 100%, and 125%) of system loading conditions. Using CPF, the maximum loading of the system with the base case is observed near the nose point. At this nose point, the bus with the least value of the voltage magnitude is considered to be the most critical bus and is a suitable location for the deployment of RE. The line stability indices Lmn, FVSI, and Lqp are evaluated for all lines of the system under different system loading scenarios. The line indices are compared with or without wind energy integration, and solar PV generation integration. It is observed that the most severe line of the system may be changed according to operating scenarios in terms of system loading. It is found that the severity of these lines gets reduced in the cases of the integration of wind energy and solar PV generation. It is also found that the maximum loadability of the system gets improved in both cases of wind energy integration and solar PV generation integration in all considered operating scenarios. The improvement in the maximum loadability and line indices are found more when solar PV generation is connected in comparison to wind energy integration in the system. However, this research work may be extended further in the following directions:

1) The researchers may develop online real-time methods for determining the voltage level of the network and the instability threshold. If the voltage instability (collapse) is identified at an early stage, it is expected that power systems can be further optimized in an effective and timely approach.
2) Dealing with the growing asynchronous generation from renewable sources: The network's escalating complexity as a result of the larger penetration of the RE resources may cause more stability problems. The probability of major disturbance instability may exponentially increase with increased DG integration. Therefore, it might be crucial to coordinate the current synchronous generation with the growing asynchronous power sources.
3) The voltage stability can be accessed with RE integration in the system under various fault scenarios.

REFERENCES

[1] I. Das, K. Bhattacharya, and C. Canizares, "Optimal incentive design for targeted penetration of renewable energy sources," *IEEE Trans. Sustainable Energy*, vol. 5, no. 4, pp. 1213–1225, 2014.

[2] I. Stoian, A. Marichescu, M. Gordan, and V. Gavrea, "Computer based modeling and simulation for wind energy systems," in *2008 IEEE Int. Conf. Autom. Qual. Test. Rob.*, vol. 3, pp. 337–342, IEEE, 2008.

[3] A. Sharif, S. A. Raza, I. Ozturk, and S. Afshan, "The dynamic relationship of renewable and nonrenewable energy consumption with carbon emission: a global study with the application of heterogeneous panel estimations," *Renewable Energy*, vol. 133, pp. 685–691, 2019.

[4] A. Ogunjuyigbe, T. Ayodele, and B. Adetokun, "Steady state analysis of wind-driven self-excited reluctance generator for isolated applications," *Renewable Energy*, vol. 114, pp. 984–1004, 2017.

[5] T. Ayodele, A. Ogunjuyigbe, and B. Adetokun, "Optimal capacitance selection for a wind-driven self-excited reluctance generator under varying wind speed and load conditions," *Appl. Energy*, vol. 190, pp. 339–353, 2017.

[6] K. Ohlenforst, S. Sawyer, A. Dutton, B. Backwel, R. Fiestas, J. Lee, L. Qiao, F. Zhao, and N. Balachandran, "Gwec global wind report 2018," *Global Wind Energy Counc. Rue dArlon*, vol. 80, p. 1040, 2019.

[7] A. Eid, M. A. Mehanna, and T. Mahmoud, "Power system stability enhancement by pv distributed generation," *J. Al-Azhar Univ. Eng. Sector*, vol. 14, no. 51, pp. 543–551, 2019.

[8] V. Khare, S. Nema, and P. Baredar, "Solar–wind hybrid renewable energy system: A review," *Renewable Sustainable Energy Rev.*, vol. 58, pp. 23–33, 2016.

[9] G. Hocine, L. Fatiha, G. Zohra, and A. Tayeb, "The interest of the wind farm of adrar to the southwest network of algeria," *Iran. J. Energy Environ.*, vol. 10, no. 3, pp. 165–170, 2019.

[10] X. Liang, H. Chai, and J. Ravishankar, "Analytical methods of voltage stability in renewable dominated power systems: a review," *Electr.*, vol. 3, no. 1, pp. 75–107, 2022.

[11] M. S. Rawat and S. Vadhera, "A comprehensive review on impact of wind and solar photovoltaic energy sources on voltage stability of power grid," *Int. J. Eng. Res.*, vol. 7, no. 4, 2019.

[12] C. Reis and F. M. Barbosa, "Line indices for voltage stability assessment," in *2009 IEEE Bucharest PowerTech*, pp. 1–6, IEEE, 2009.

[13] R. Fadaeinedjad, G. Moschopoulos, and M. Moallem, "A new wind power plant simulation method to study power quality," in *2007 Can. Conf. Electr. Comput. Eng.*, pp. 1433–1436, IEEE, 2007.

[14] A. A. Tamimi, A. Pahwa, S. Starrett, and N. Williams, "Maximizing wind penetration using voltage stability based methods for sizing and locating new wind farms in power system," in *IEEE PES Gen. Meet.*, pp. 1–7, IEEE, 2010.

[15] A. Melo, S. Granville, J. Mello, A. Oliveira, C. Domellas, and J. Soto, "Assessment of maximum loadability in a probabilistic framework," in *IEEE Power Eng. Soc. 1999 Winter Meet. (Cat. No. 99CH36233)*, vol. 1, pp. 263–268, IEEE, 1999.

[16] P. Kundur, "Power system stability," *Power Syst. Stab. Control*, vol. 10, pp. 7–1, 2007.

[17] P. Kundur, J. Paserba, V. Ajjarapu, G. Andersson, A. Bose, C. Canizares, N. Hatziargyriou, D. Hill, A. Stankovic, C. Taylor, *et al.*, "Definition and classification of power

system stability ieee/cigre joint task force on stability terms and definitions," *IEEE Trans. Power Syst.*, vol. 19, no. 3, pp. 1387–1401, 2004.

[18] M. S. Rawat and S. Vadhera, "Probabilistic steady state voltage stability assessment method for correlated wind energy and solar photovoltaic integrated power systems," *Energy Technol.*, vol. 9, no. 2, p. 2000732, 2021.

[19] B. B. Adetokun, C. M. Muriithi, J. O. Ojo, and O. Oghorada, "Impact assessment of increasing renewable energy penetration on voltage instability tendencies of power system buses using a qv-based index," *Sci. Rep.*, vol. 13, no. 1, p. 9782, 2023.

[20] M. Kazeminejad, M. Banejad, U. Annakkage, and N. Hosseinzadeh, "The effect of high penetration level of distributed generation sources on voltage stability analysis in unbalanced distribution systems considering load model," *J. Oper. Autom. Power Eng.*, vol. 7, no. 2, pp. 196–205, 2019.

[21] R. Kyomugisha, C. M. Muriithi, and M. Edimu, "Multiobjective optimal power flow for static voltage stability margin improvement," *Heliyon*, vol. 7, no. 12, 2021.

[22] S. Gupta, J. Tripathi, A. Ranjan, R. Kesh, A. Kumar, M. Ranjan, and P. Sahu, "Optimal sizing of distributed power flow controller based on jellyfish optimizer," *J. Oper. Autom. Power Eng.*, vol. 12, no. 1, pp. 69–76, 2024.

[23] W. Tang, W. Li, J. Zheng, C. Wu, L. Wang, Q. Wei, and Q. Wu, "A composite voltage stability index for integrated energy systems based on l-index and the minimum eigenvalue of reduced jacobian matrix," *Int. J. Electr. Power Energy Syst.*, vol. 141, p. 108136, 2022.

[24] B. Ismail, N. I. A. Wahab, M. L. Othman, M. A. M. Radzi, K. N. Vijayakumar, M. K. Rahmat, and M. N. M. Naain, "New line voltage stability index (bvsi) for voltage stability assessment in power system: the comparative studies," *IEEE Access*, vol. 10, pp. 103906–103931, 2022.

[25] M. Mohammadniaei, F. Namdari, and M. Shahkarami, "A fast voltage collapse detection and prevention based on wide area monitoring and control," *J. Oper. Autom. Power Eng.*, vol. 8, no. 3, pp. 209–219, 2020.

[26] Q. Wang, Y. Zhang, P. Tian, B. Ren, Q. Li, P. Luo, and J. Hao, "Research on the influence of load model with distributed pv generation on the voltage stability of receiving-end power grid," *Energy Rep.*, vol. 9, pp. 880–886, 2023.

[27] M. Glavic and S. Greene, "Voltage stability in future power systems," 2023.

[28] G. Rui-peng and H. Zhen-xiang, "An improved zero eigen value method for point of collapse," *Proc.-Chin. Soc. Electr. Eng.*, vol. 20, no. 5, pp. 63–66, 2000.

[29] D. Xianzhong, H. Yangzan, and C. Deshu, "On some practical criteria and security indices for voltage stability in electric power system," *Autom. Electr. Power Syst.*, vol. 18, no. 9, pp. 36–41, 1994.

[30] M. Moghavvemi and F. Omar, "Technique for contingency monitoring and voltage collapse prediction," *IEE Proc.-Gener. Transm. Distrib.*, vol. 145, no. 6, pp. 634–640, 1998.

[31] I. Musirin and T. A. Rahman, "On-line voltage stability based contingency ranking using fast voltage stability index (fvsi)," in *IEEE/PES Transm. Distrib. Conf. Exhibition*, vol. 2, pp. 1118–1123, IEEE, 2002.

[32] S. Ratra, R. Tiwari, and K. R. Niazi, "Voltage stability assessment in power systems using line voltage stability index," *Comput. Electr. Eng.*, vol. 70, pp. 199–211, 2018.

[33] A. Mohamed, G. Jasmon, and S. Yusoff, "A static voltage collapse indicator using line stability factors," *J. Ind. Technol.*, vol. 7, no. 1, pp. 73–85, 1989.

[34] A. Chebbo, M. Irving, and M. Sterling, "Voltage collapse proximity indicator: behaviour and implications," in *IEEE Proc. C (Gener. Transm. Distrib.)*, vol. 139, pp. 241–252, IET, 1992.

[35] T. An, S. Zhou, J. Yu, and Y. Zhang, "Tracking of thevenin equivalent parameters on weak voltage load bus groups," in *2006 IEEE PES Power Syst. Conf. Exposition*, pp. 1570–1576, IEEE, 2006.

[36] R.-A. Moradi and R. Z. Davarani, "Introducing a new index to investigate voltage stability of power systems under actual operating conditions," *Int. J. Electr. Power Energy Syst.*, vol. 136, p. 107637, 2022.

[37] A. Yazdanpanah-Goharrizi and R. Asghari, "A novel line stability index (nlsi) for voltage stability assessment of power systems," in *Proc. 7th WSEAS Int. Conf. Power Syst.*, pp. 164–167, Citeseer, 2007.

[38] A. Alshareef, R. Shah, N. Mithulananthan, and S. Alzahrani, "A new global index for short term voltage stability assessment," *IEEE Access*, vol. 9, pp. 36114–36124, 2021.

[39] A. Alshareef, R. Shah, N. Mithulananthan, and S. Alzahrani, "A new global index for short term voltage stability assessment," *IEEE Access*, vol. 9, pp. 36114–36124, 2021.

[40] R. D. Christie, "Ieee 14-bus and ieee 118-bus systems," 1999. Accessed on August, 1999.

[41] H.-D. Chiang, A. J. Flueck, K. S. Shah, and N. Balu, "Cpflow: A practical tool for tracing power system steady-state stationary behavior due to load and generation variations," *IEEE Trans. Power Syst.*, vol. 10, no. 2, pp. 623–634, 1995.

[42] M. Karimi, A. Shahriari, M. Aghamohammadi, H. Marzooghi, and V. Terzija, "Application of newton-based load flow methods for determining steady-state condition of well and ill-conditioned power systems: A review," *Int. J. Electr. Power Energy Syst.*, vol. 113, pp. 298–309, 2019.

[43] B. B. Adetokun, C. M. Muriithi, and J. O. Ojo, "Voltage stability assessment and enhancement of power grid with increasing wind energy penetration," *Int. J. Electr. Power Energy Syst.*, vol. 120, p. 105988, 2020.

[44] B. Spichartz, K. Günther, and C. Sourkounis, "New stability concept for primary controlled variable speed wind turbines considering wind fluctuations and power smoothing," *IEEE Trans. Ind. Appl.*, vol. 58, no. 2, pp. 2378–2388, 2022.

[45] B. B. Adetokun, A. Adekitan, T. Somefun, A. Aligbe, and A. Ogunjuyigbe, "Artificial neural network-based capacitance prediction model for optimal voltage control of stand-alone wind-driven self-excited reluctance generator," in *2018 IEEE PES/IAS PowerAfr.*, pp. 485–490, IEEE, 2018.

[46] M. Mohammadniaei, F. Namdari, and M. Shahkarami, "A fast voltage collapse detection and prevention based on wide area monitoring and control," *J. Oper. Autom. Power Eng.*, vol. 8, no. 3, pp. 209–219, 2020.

[47] P. Akbarzadeh Aghdam and H. Khoshkhoo, "Voltage stability assessment algorithm to predict power system loadability margin," *IET Gener. Trans. Distrib.*, vol. 14, no. 10, pp. 1816–1828, 2020.

[48] P. Kumar, N. Pal, and H. Sharma, "Optimization and techno-economic analysis of a solar photo-voltaic/biomass/diesel/battery hybrid off-grid power generation system for rural remote electrification in eastern india," *Energy*, vol. 247, p. 123560, 2022.

[49] U. E. Uzun, N. Pamuk, and S. Taskin, "Effect of solar photovoltaic generation systems on voltage stability," in *2022 Global Energy Conf. (GEC)*, pp. 38–41, IEEE, 2022.

[50] S. Rahman, S. Saha, S. N. Islam, M. T. Arif, M. Mosadeghy, M. Haque, and A. M. Oo, "Analysis of power grid voltage stability with high penetration of solar pv systems," *IEEE Trans. Ind. Appl.*, vol. 57, no. 3, pp. 2245–2257, 2021.

[51] S. Kumar, A. Kumar, and N. Sharma, "A novel method to investigate voltage stability of ieee-14 bus wind integrated system using psat," *Front. Energy*, vol. 14, pp. 410–418, 2020.

[52] B. B. Adetokun, C. M. Muriithi, and J. O. Ojo, "Voltage stability assessment and enhancement of power grid with increasing wind energy penetration," *Int. J. Electr. Power Energy Syst.*, vol. 120, p. 105988, 2020.

APPENDIX

The system parameters of IEEE 14-bus and 118-bus systems are available online in [40].

Table A1. Simulation system data of IEEE 14-bus system.

From Bus	To Bus	Resistance (in p.u.)	Reactance (in p.u.)	Impedance angle (in degrees)
4	9	0.0000	0.5562	90.0000
14	13	0.1709	0.3480	63.8420
9	14	0.1271	0.2704	64.8210
6	12	0.1229	0.2558	64.3369
5	6	0.0000	0.2520	90.0000
5	1	0.0540	0.2230	76.3828
4	7	0.0000	0.2091	90.0000
12	13	0.2209	0.1999	42.1376
6	11	0.0950	0.1989	64.4743
3	2	0.0470	0.1980	76.6474
11	10	0.0821	0.1921	66.8684
2	4	0.0581	0.1763	71.7593
8	7	0.0000	0.1762	90.0000
2	5	0.0570	0.1739	71.8651
3	4	0.0670	0.1710	68.6046
6	13	0.0662	0.1303	63.0789
7	9	0.0000	0.1100	90.0000
9	10	0.0318	0.0845	69.3712
1	2	0.0194	0.0592	71.8648
5	4	0.0134	0.0421	72.4100

Table A2. Simulation data information of IEEE 14-bus and IEEE 118-bus systems.

System parameters	IEEE 14-bus system at base case loading (in p.u.)	IEEE 118-bus system at base case loading (in p.u.)
PSAT version used for simulation	2.1.11	
Total real power generation	7.610424	151.6911
Total generation of reactive power	7.655304	208.893
Total loads of real power	6.143219	124.3596
Total loads of reactive power	1.930726	50.56763
Wind energy stator side-resistance and reactance	0.01 and 0.08	0.01 and 0.08
Wind energy rotor side-resistance and reactance	0.01 and 0.08	0.01 and 0.08
Speed of the wind	15 m/s	15 m/s
Solar PV generator (PV)	40 MW	100 MW